NASA TECHNICAL MEMORANDUM

NASA TM X-71505

NASA TM X-71505

SUMMARY OF RECENT INVESTIGATIONS OF INLET FLOW DISTORTION EFFECT ON ENGINE STABILITY

by Edwin J. Graber, Jr. and Willis M. Braithwaite
Lewis Research Center
Cleveland, Ohio 44135

TECHNICAL PAPER proposed for presentation at
Twelfth Aerospace Sciences Meeting sponsored by
the American Institute of Aeronautics and Astronautics
Washington, D.C., January 30 - February 1, 1974

ABSTRACT

A review is presented of recent experimental results, analytical procedures and test techniques employed to evaluate the effects of inlet flow distortion on the stability characteristics of representative afterburning turbofan and turbojet compression systems. Circumferential distortions of pressure and temperature, separately and in combination, are considered. Resulting engine sensitivity measurements are compared with predictions based on simplified parallel compressor models and with several distortion descriptor parameters.

SUMMARY OF RECENT INVESTIGATIONS OF INLET FLOW DISTORTION EFFECT ON ENGINE STABILITY

by Edwin J. Graber, Jr. and Willis M. Braithwaite

NASA-Lewis Research Center

Cleveland, Ohio

E-7878

INTRODUCTION

In the development of an airbreathing propulsion system allowances must be made for the effects of inlet flow non-uniformities on engine stability. These flow distortions are detectable at the engine-inlet interface plane as variations in temperature and/or pressure. There are many factors which can contribute to the formation of such distortions. Typically, pressure distortions result from operation at high angles of attack and/or yaw, from wakes from nearby aircraft, and through inlet boundary layer interactions. Temperature distortions may result from armament firing or the ingestion of hot exhaust gases from thrust reversers, from steam driven catapults used on aircraft carriers, or from the exhaust plumes of nearby aircraft. In addition, temperature distortions or combined pressure and temperature distortions may enter intermediate or aft compressors in the more complex two and three spool compressor systems as the result of inlet pressure distortions. Increasing the design compressor surge margin to accommodate these unknown inlet distortions may result in an arbitrary reduction of engine performance accompanied by an increase in engine weight. Thus, the allocation of surge margin required for inlet distortions must be assessed as closely as possible without compromising engine stability.

During the past several years, NASA Lewis Research Center has been conducting a program to determine the effect of inlet flow distortions (both temperature and pressure) on the stability of several gas turbine engines (e.g., refs. 1 through 13). This paper is an extension of ref. 1 and presents the results of the steady-state circumferential temperature and pressure distortion tests conducted on two representative gas turbine engines; - - a simple one-spool turbojet (J85-GE-13) and a two-spool turbofan (TF30-P-3). Both the empirical approach of employing a distortion index to establish the distortion sensitivity or the stability limit of an engine and a comparison with the predicted results using parallel compressor theory are presented.

Apparatus and Procedure

For the J-85 engine, surge data was obtained for circumferential pressure distortions of 60^{o}, 90^{o}, and 180^{o} extents; temperature distortions of 90^{o}, 180^{o}, and 270^{o} extents; and combined pressure and temperature distortions of 180^{o} extent each, arranged with 0^{o}, 90^{o}, and 180^{o} of overlap. Pressure distortions were created by placing screens of various porosities and extents in the inlet duct approximately one duct diameter upstream of the engine face. The resulting pressure distribution at the engine-inlet interface plane was measured using six evenly spaced total pressure rakes of five elements each. Temperature distortions were generated using a gaseous hydrogen burner (ref. 4) located approximately four inlet duct diameters upstream of the engine face. This burner was divided into four 90^{o} quadrants each controlled independently through the regulation of its hydrogen flow rate. Twelve rakes of five thermocouples each and four rakes of two total pressure probes each were used to measure the resulting distortion patterns at the interface plane. The details of the installation, instrumentation, engine modifications made, and testing procedures are given in ref. 3 for the pressure distortion tests and in ref. 4 for the temperature distortion tests. Engine surge in both cases was induced by gradually reducing the exhaust nozzle area and thus increasing the compressor back pressure at a constant rotor speed until stall occurred.

The TF30 data includes circumferential pressure distortions of 120^{o}, 180^{o}, 240^{o}, and 300^{o} extents and temperature distortions of 90^{o}, 180^{o}, and 270^{o} extents. The pressure distortions were generated using the air-jet system described in ref. 5. Basically, this system consists of a series of forward facing air jets. By flowing high pressure air through some of the jets, the desired flow pattern was created. Increasing these flow rates increased the amplitude of the distortion. Pressure distributions at the inlet-engine interface were measured using eight equally spaced total pressure rakes of five probes each. The temperature distortions were generated using the hydrogen burner as for the J-85. Resulting distortion patterns at the inlet-engine interface were measured using sixteen equally spaced rakes, eight with five thermocouples each and eight with two thermocouples and five total pressure probes each (see ref. 2). Details of the installation, instrumentation, and testing procedures are presented in ref. 6 for the pressure distortion tests and in ref. 2 for the temperature distortion tests. Engine surge was induced in both cases by increasing the amplitude of the inlet flow distortion until surge occurred.

Data Correlation with Distortion Indices

One approach to the problem of relating the severity of the inlet flow distortion to the resulting loss on surge margin is through the use of distortion indices. A wide variety of pressure distortion indices are in use throughout the industry today (e.g., refs. 14 through

19). The resulting variations in the form of the indices has made it extremely difficult to compare the work of different investigators. In this paper, the subject J85 and TF-30 data are presented and compared in terms of the basic $\Delta P/P$ (i.e., $(P_{ave} - P_{min})/P_{ave}$) and $\Delta P/Q$ (i.e., $(P_{ave} - P_{min})/Q_{ave}$) forms which are related to the more commonly used indices noted in Table I for the basic square wave circumferential distortion patterns considered herein. This was done in order to show the degree of data correlation achieved with as little confusion as possible. The relationships of Table I can be used to calculate an approximate value of any of the listed indices from the data presented. Although the actual circumferential profiles are not perfectly square, a reasonable approximation to the index should result.

One interesting observation can be made from Table I. The weighting of the extent of the distortion term, $\bar{\Theta}$, varies considerably from index to index. Since many of the indices cited were developed for and presumably best correlate the stall data of a specific engine design, it appears that a fixed weighting of the extent term in any universally applied distortion index is not a reasonable goal.

The authors know of no temperature distortion index which has been developed and substantiated by a significant quantity of data. Thus, the basic $\Delta T/T$ (i.e., $(T_{max} - T_{ave})/T_{ave}$) parameter will be used in this paper. In addition, a speed correction to this term which is implied by parallel compressor theory will be presented.

As with the distortion indices, there are several ways to evaluate the loss in surge pressure ratio due to distortion (i.e. ΔPRS). Two of these methods are presented since they are the most commonly employed definitions. The first definition of ΔPRS is given as the percentage loss in surge pressure ratio at a constant corrected airflow. Referring to figure 1, the calculation becomes:

$$\Delta PRS_W = \left(\frac{PR_B - PR_A}{PR_B} \right) \times 100 \qquad (1)$$

All symbols are defined in the Symbol List at the end of the paper. The other definition is the percentage loss in surge pressure ratio at a constant corrected speed, or in terms of the nomenclature of fig. 1:

$$\Delta PRS_N = \left(\frac{PR_C - PR_A}{PR_C} \right) \times 100 \qquad (2)$$

This definition is the one suggested by the parallel compressor theory as will be shown later in the paper. The data will be presented using both definitions.

Parallel Compressor Model

The parallel compressor model used herein to predict the loss in surge pressure ratio for the J85 and the TF-30 is the same as that presented in ref. 1. A review of this model is presented below.

Parallel Compressor Theory

In parallel compressor theory, it is assumed that for distorted inlet flow, the compressor may be segmented into a series of sub-compressors each operating independently of one another and each assumed to have the same performance characteristics as the undistorted compressor. Since they all discharge into a common plenum, their exit static pressures are assumed identical. Compressor surge is then assumed to occur when any one of these sub-compressors reaches its undistorted surge pressure ratio.

For the J85 engine, an additional assumption was added based on experimental results. The compressor exit total pressure was observed to be uniform at the compressor exit plane. This non-standard assumption for parallel compressor theory simplified its application. The eventual result is a relatively simple relationship between the loss in surge pressure ratio to the basic $\Delta P/P$ and $\Delta T/T$ parameters. More detailed discussion is provided in a subsequent section.

Application of the Model

The general application of the parallel compressor model to a simple one-spool turbojet engine such as the J85 is illustrated in fig. 2. Shown in this figure are the compressor maps required for the parallel compressor analysis and a cross-section of the compressor inlet illustrating the distortion pattern being considered. Here, the undistorted quadrant is labeled as quadrant "1" and its corresponding operating point (sub-compressor number one) is located on the upper map. Adding a pressure distortion (pressure decrement) moves the operating point along a constant corrected speed line to point "2" on the map. This corresponds to the operating point of sub-compressor number two. Next, imposing a temperature distortion (temperature increment) results in a shift from point "2" to point "3" at a constant exit static-to-inlet total pressure ratio to a lower corrected speed (sub-compressor

number three). The alternate path from "1" to "4" to "3" could be traced in a similar manner by first imposing a temperature and then a pressure distortion. Corresponding operating points on the compressor performance map based on an exit total-to inlet total pressure ratio (lower curve) are found using the corrected airflows and corrected speeds from the upper curve.

It should be noted that in practice, it is first assumed which sub-compressor is operating at the surging condition, since according to the theory, compressor surge occurs when any of the sub-compressors operates on its clean inlet surge line. This point is found as the intersection of the surge line and the corrected speed line. Knowing the spatial variation in inlet total temperature and pressure at the surge point enables the determination of each of the remaining sub-compressor operating points. Each of these sub-compressors should then be operating below the surge line. If this is not the case, then the initial guess as to the critical sub-compressor is in error and a new critical sub-compressor then has to be selected and the procedure repeated.

The parallel compressor model was also applied to the TF-30, a two-spool turbofan engine, for the temperature distortions. This compressor was divided into three units: a three-stage fan and a nine- (3+6) stage low pressure compressor on one spool and a seven-stage high pressure compressor on the other spool. The fan was considered to be the tip portion of the first three stages and the low pressure compressor, the hub portion of the three-fan stages plus the next six low compressor stages. The parallel compressor solutions for the three compressor units were established using experimentally measured exit static-to-inlet total pressure ratios across each unit. In each case, the assumption of constant exit static pressure was verified by the experimental data.

Simplified Model

As previously noted, a simplification of the parallel compressor model was developed in ref. 1 specifically for the J85 engine. In addition to the usual assumptions of the parallel compressor theory, the following assumptions were made:

1. The compressor exit total pressure is uniform.

2. The compressor surge pressure ratio varies linearly with corrected speed over the range of interest, i.e.,

$$PRS = AN/\sqrt{\theta} + B \qquad (3)$$

3. The distortions were small enough in amplitude to allow second order difference terms and higher to be neglected (i.e., terms such as $(\Delta T/T)^2$, $(\Delta P/P)^2$, $(\Delta T/T)\times(\Delta P/P)$, etc.).

It was found that for the general case of combined temperature and pressure distortions, the loss in surge pressure ratio is given by

$$\Delta PRS_N = \frac{\Delta P}{P} + \frac{\frac{1}{2}\frac{\Delta T}{T}}{1 + \frac{B}{AN/\sqrt{\theta_{ave}}}} \tag{4}$$

where

$$\frac{\Delta P}{P} = \frac{P_{ave} - P_k}{P_{ave}} \tag{5}$$

and

$$\frac{\Delta T}{T} = \frac{T_k - T_{ave}}{T_{ave}} \tag{6}$$

Here, k indicates the condition at the inlet to the sub-compressor which induced the surge. For the case of overlapping temperature and pressure distortions, it was determined that surge always originates in the region where $P_k = P_{min}$ and $T_k = T_{max}$ (i.e., the overlapped region-quadrant 3 in fig. 2). For non-overlapping patterns, $P_k = P_{max}$ and $T_k = T_{max}$ if surge is induced in the temperature distortion region. Conversely, $P_k = P_{min}$ and $T_k = T_{min}$ if surge is induced in the pressure distortion region. The loss in surge pressure ratio, ΔPRS_N, in this case is the larger of these two calculated ΔPRS_N values. Pressure distortion only and temperature distortion only thus become specific cases with $\Delta T/T = 0$ and $\Delta P/P = 0$, respectively

Results and Discussion

The results of applying both the reduced distortion indices and the parallel compressor theory to the pressure and temperature distortion surges of both the J-85 and TF30 engines are discussed below.

Turbojet Engine (J-85)

Consider first the results of the pressure distortion surge tests. The loss in surge pressure ratio evaluated at a constant corrected speed, ΔPRS_N, as a function of the amplitude of the distortion pattern (i.e. $\Delta P/P$) for the circumferential distortion patterns tested is shown in figure 3. Also shown is the parallel compressor prediction. As can be seen, the predicted relationship between ΔPRS_N and $\Delta P/P$ is a reasonable one for this engine.

Evaluating the loss in surge pressure ratio at a constant corrected airflow, ΔPRS_W, and maintaining the same measure of the distortion amplitude (i.e. $\Delta P/P$) resulted in a marked scattering of the data (figure 4). For this definition, sizeable corrections for the effect of extent and corrected speed would be required to reduce the data to one curve. However, to accurately determine these corrections, it would be necessary to obtain considerably more surge data.

Using a $\Delta P/Q$ parameter with either ΔPRS_N or ΔPRS_W (figures 5 and 6 respectively) does not appear to offer any improvement in the degree of data correlation. Trends due to the extent of the distortion and the corrected speed appear to be present but would require additional data to determine accurately.

Next, consider the results of the temperature distortion tests. The loss in surge pressure ratio as a function of the basic $\Delta T/T$ parameter is shown in figures 7 and 8 for the two definitions of ΔPRS. Neither ΔPRS definition appears to offer a simple relationship for all extents and speeds or to offer an advantage over the other. Although the data appear to separate into two linear groups in both figures, neither the extent of distortion nor the corrected speed is common to either group. The speed correction implied by the simplified parallel compressor model (equation 4) is applied to the basic $\Delta T/T$ parameter in figure 9. For extents greater than 90°, the data agree fairly well with parallel compressor predictions while the 90° extent data fall along a line parallel to but to the right of the predicted values. It is possible that the values of $\Delta T/T$ calculated in this case should be corrected due to the circumferential profile shape. As can be seen in figure 10, the temperature distribution for the 90° extent distortion case deviated considerably from the ideal square wave pattern assumed in the parallel compressor model. There is also the possibility that the 90° extent is less than some minimum extent similar to the minimum extent found for the case of pressure distortions, noted in references 3 and 20.

Although the combined pressure and temperature distortion data are discussed in reference 1, the data will also be re-presented here for the sake of completeness. A comparison of the experimentally determined and predicted (using parallel compressor theory) ΔPRS_N values is shown in figure 11. It appears that the parallel compressor model yields a reasonable estimate of the effect of combined distortions on the engine stability.

Turbofan Engine (TF30)

In evaluating the effect of inlet flow distortions on the turbofan engine, the interface conditions between the three compressor units must not be altered by the test technique. Therefore, the technique of raising the operating point by increasing compressor back pressure such as was done in the J-85 testing was not used. Instead, the minimum distortion level was found which would induce compressor surge by slowly increasing the amplitude of distortion while keeping the engine variables such as bleeds and nozzle area in the standard position. The results of the pressure distortion - engine surge tests in terms of the limiting $\Delta P/P$ and $\Delta P/Q$ values are shown in figures 12a and 12b respectively. A log-log plot of either $\Delta P/P$ or $\Delta P/Q$ versus the extent of distortion (figs. 13a and 13b) indicates that the weighting factor for extent which would reduce these data to one curve is simply θ^{-} in both cases. This weighting is included in both the K_{D2} and K_{θ} indices (see Table I) which were developed specifically for this engine design.

Limiting levels of temperature distortion in terms of $\Delta T/T$ at surge are plotted in figure 14 as a function of engine corrected speed. No simple weighting of the extent term could be determined from a log-log plot of $\Delta T/T$ versus extent.

As might be expected the distortion levels required to surge the engine for either temperature or pressure distortions decreased as the angular extent of distortion increased. For the 180° extent pressure distortions, at 90% corrected speed, about 6.4% $\Delta P/P$ was required to induce surge. In comparison, for the temperature distortions, at 90% corrected speed, about 8.1% $\Delta T/T$ resulted in engine surge. Thus, the TF30 was slightly more sensitive to pressure distortions than to temperature distortions.

As mentioned previously, a parallel compressor model was applied to the TF30 temperature distortion data and typical results for a 180° extent pattern are shown in figure 15. As seen in figure 15a, neither of the fan's parallel subcompressors is operating close to the surge line. However, for both the low pressure compressor and the high pressure compressor units, one of their subcompressors is operating near the surge line (figs. 15b and 15c). These results imply that both units are critical. Examination of time histories of the inlet and exit pressures of each unit (see ref. 2) indicates that the low pressure compressor developed rotating stall which was followed by complete flow breakdown in the high pressure compressor. Thus, the parallel compressor model was found to be a useful tool for understanding the behavior of the more complex compressor systems such as the TF30.

Summary of Results

1. The J-85 pressure distortion surges can be predicted reasonably well using the parallel compressor theory. As indicated by the theory, defining the loss of compressor surge pressure ratio at a constant corrected speed results in the best correlation with $\Delta P/P$.

2. The J-85 temperature distortion surges are predicted reasonably well for the above 90^{o} extent distortion patterns. There is, however, disagreement for the 90^{o} extent data which may be attributable to the pattern shape.

3. Correlation of the loss in surge pressure ratio with the basis $\Delta T/T$ parameter for the J-85 revealed no advantage in using either a constant corrected speed or constant corrected airflow definition of ΔPRS.

4. Combined pressure and temperature distortion effects on the surge pressure ratio of the J-85 were in reasonable agreement with the parallel compressor model.

5. The stability limit of the TF30 engine could be correlated using either $((\Delta P/P) \cdot \Theta^{-})$ or $((\Delta P/Q) \cdot \Theta^{-})$ for the pressure distortion induced surge data.

6. The TF30 was slightly more sensitive to pressure than to temperature distortions.

7. Parallel compressor theory was found to be a useful tool in analyzing surge data for both engines.

Symbols

A	Slope of corrected rotor speed vs. surge pressure ratio line, $\Delta(PR) \div \Delta(N/\sqrt{\theta})$, equation 3.
B	Intercept of corrected rotor speed vs. surge pressure ratio line, equation 3.
N	Compressor rotor speed, RPM
P	Total pressure
Δ P/P	$(P_{ave} - P_{min})/P_{ave}$
P_S	Static pressure
PR	Compressor pressure ratio
PRS	Compressor pressure ratio at surge
Δ PRS	Loss in surge pressure ratio, equations 1 and 2
Q	Dynamic head
T	Total temperature
$\frac{\Delta T}{T}$	$(T_{max} - T_{ave})/T_{ave}$
W	Mass flow rate of air
δ	Ratio of compressor inlet total pressure to standard ambient sea-level total pressure
θ	Ratio of compressor inlet total temperature to standard ambient sea-level total temperature.
$\bar{\theta}$	Circumferential extent of the below average pressure region.
ϕ	Circumferential extent over which pressures are averaged.

Subscripts

ave	average
c	core
F	fan exit
H	high pressure compressor

Subscripts (cont'd)

in	compressor inlet
k	critical sub-compressor in parallel compressor theory
L	low pressure compressor
min	average of below face average quantity
max	average of above face average quantity
N	evaluated at constant corrected speed
out	compressor exit
w	evaluated at constant corrected airflow
2	fan or low pressure compressor inlet
3	low pressure compressor exit or high pressure compressor inlet
4	high pressure compressor exit

References

1. Braithwaite, W. M.; Graber, E. J. Jr.; and Mehalic, C. M.: The Effects of Inlet Temperature and Pressure Distortion on Turbojet Performance. Paper 73-1316, AIAA, November 1973.

2. Braithwaite, W. M.: Experimental Evaluation of a TF30-P-3 Turbofan Engine in an Altitude Facility: Effect of Steady-State Temperature Distortion. NASA TM X-2921, November 1973.

3. Calogeras, J. E.; Mehalic, C. M.; and Burstadt, P. L.: Experimental Investigation of the Effect of Screen-Induced Total-Pressure Distortion on Turbojet Stall Margin. NASA TM X-2239, March 1971.

4. Mehalic, C. M. and Lottig, R. A.: Steady State Inlet Temperature Distortion Effects on the Stall Limit of a J85-GE-13 Turbojet Engine. NASA TM X-2990, 1974.

5. Braithwaite, W. M.; Dicus, J. H.; and Moss, J. E. Jr.: Evaluation with a Turbofan Engine of Air Jets as a Steady-State Inlet Flow Distortion Device. NASA TM X-1955, January 1970.

6. McAulay, J. E. and Abdelwahab, M.: Experimental Evaluation of a TF30-P-3 Turbofan Engine in an Altitude Facility: Afterburner Performance and Engine-Afterburner Operating Limits. NASA TN D-6839, July 1972.

7. Povolny, J. H.: Stall and Distortion Investigation of a YTF30-P-1 Turbofan Engine. NASA TM X-52622, June 1969.

8. Rudey, R. A.; and Antl, R. J.: The Effect of Inlet Temperature Distortion on the Performance of a Turbo-Fan Engine Compressor System. NASA TM X-52788, 1970.

9. Straight, D. M. and Mehalic, C. M.: Performance and Stall Characteristics of an Afterburning Turbofan Engine with Steady-State Inlet-Flow Distortion. NASA TM X-1898, August 1970.

10. McAulay, J. E.: Effect of Dynamic Variations in Engine-Inlet Pressure on the Compressor System of a Twin-Spool Turbofan Engine. NASA TM X-2081, September 1970.

11. Antl, R. J.; Smith, J. M.; and Riddlebaugh, S.: The Effect of Screen-Induced Inlet-Flow Distortions on the Performance and Stall Characteristics of an Afterburner Equipped Turbofan Engine. NASA TM X-2242, March 1971.

12. Braithwaite, W. M. and Vollmar, W. R.: Performance and Stall Limits of a YTF30-P-1 Turbofan Engine with Uniform Inlet Flow. NASA TM X-1803, June 1969.

13. Werner, R. A.; Abdelwahab, M.; and Braithwaite, W. M.: Performance and Stall Limits of an Afterburner-Equipped Turbofan Engine with and without Inlet Flow Distortion. NASA TM X-1947, April 1970.

14. Anon.: Model TF30-P-3 Engine (JTF10A-21). Specification A-1809-A, Pratt and Whitney Aircraft, November 15, 1967.

15. Plourde, G. A. and Brimelow, B.: Pressure Fluctuations Cause Compressor Instability. Proceedings of the Air Force Airframe-Propulsion Compatibility Symposium, AFAPL-TR-69-103. Wright Patterson AFB, Ohio, June 1970.

16. Moore, M. T.: Distortion Data Analysis. AFAPL TR-72-111, February 1973.

17. Alford, J. S.; Davies, D. P.; and Young, C. C.: Inlet Duct-Engine Airflow Match and Compatibility for Supersonic Aircraft. SAE Paper No. 586C, Los Angeles, California, October 8-12, 1962.

18. ATF3 Staff: XF104-GA-100 Engine PFRT Program (Garrett Engine Model ATF3) Test Plan, Altitude Test, YF104-GA-100 Engine SN 16, AF Contract No. F33657-71-C-0996, Document No. 72-8151-1.1, December 18, 1972.

19. Williams, D. D.: Some Aspects of Inlet/Engine Compatibility, ICAS Paper No. 72-19. The Eighth Congress of the International Council of the Aeronautical Sciences, Netherlands, August 28 to September 2, 1972.

20. Reid, C.: The Response of Axial Flow Compressors to Intake Flow Distortion, Paper 69-GT-29, March 1969, ASME, New York, N.Y.

TABLE I

REDUCED FORM OF DISTORTION INDICES FOR A SQUARE-WAVE CIRCUMFERENTIAL DISTORTION PATTERN OF EXTENT $\bar{\theta}$

INDEX	REFERENCE	REDUCED FORM
K_{D_2}	14	$\frac{\Delta P}{P} \cdot \frac{\bar{\theta}}{2\pi} \cdot 36\,000$
K_θ	15	$\frac{\Delta P}{Q} \cdot \frac{\bar{\theta}}{2\pi} \cdot 2.48$
IDC	16	$\frac{\Delta P}{P} \cdot f(\bar{\theta})$
NDI	17	$\frac{\Delta P}{P} \frac{2\pi}{2\pi - \bar{\theta}} \sqrt{\frac{\bar{\theta}}{2}}$
METHOD "D"	16	$\frac{\Delta P}{P} \cdot f(\bar{\theta}, N/\sqrt{\theta})$
D. I.	18	$\frac{\Delta P}{P} \cdot \frac{\bar{\theta}}{2\pi}$
DC(φ)	19	$\frac{\Delta P}{Q}$ FOR $\varphi \leq \bar{\theta}$
		$\frac{\Delta P}{Q} \cdot \frac{\bar{\theta}}{\varphi}\left(\frac{2\pi - \varphi}{2\pi - \bar{\theta}}\right)$ FOR $\varphi > \bar{\theta}$

CS-69017

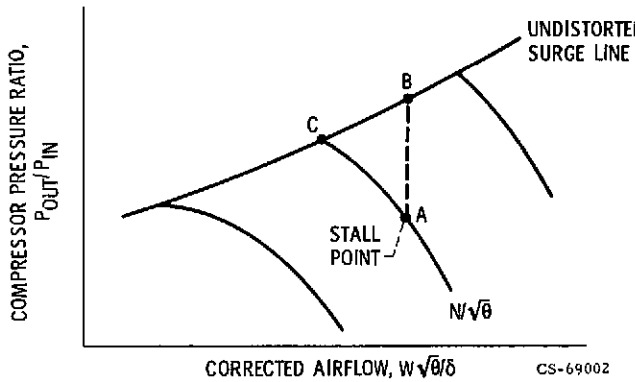

Figure 1. - Typical compressor performance map.

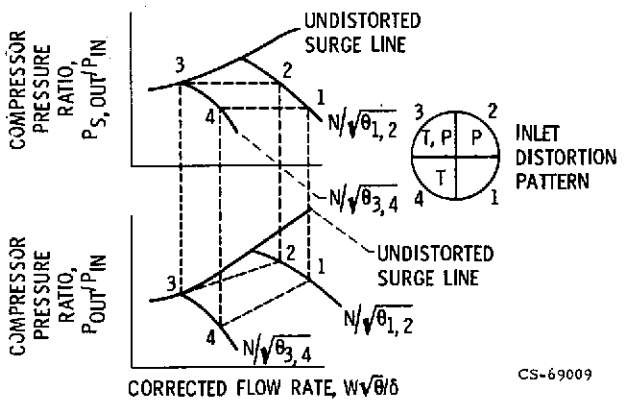

Figure 2. - Compressor performance maps required to apply parallel compressor to pressure and/or temperature distortions.

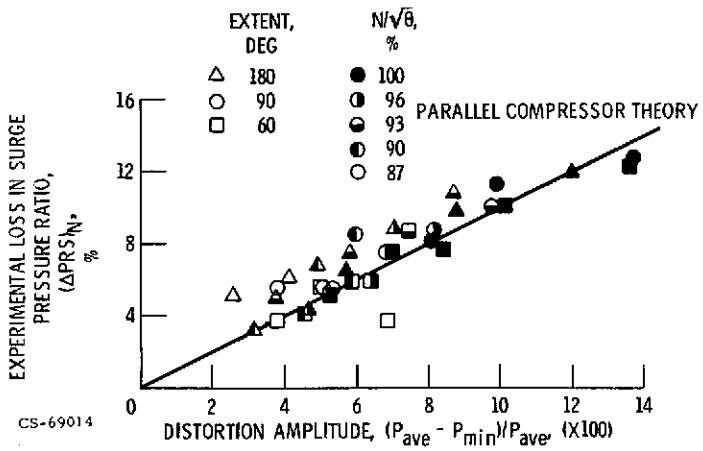

Figure 3. - J-85 circumferential pressure distortions.

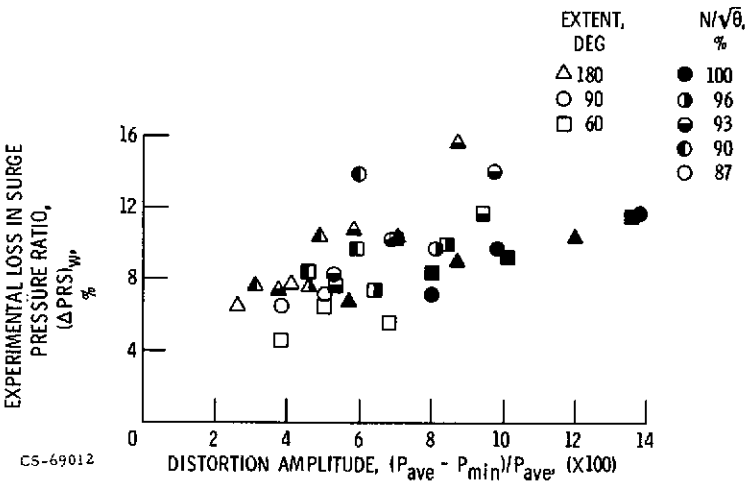

Figure 4. - J-85 circumferential pressure distortions.

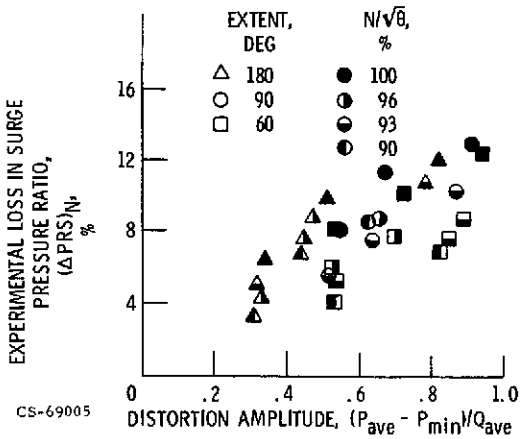

Figure 5. - Loss in J-85 surge pressure ratio (evaluated at a constant corrected speed) due to circumferential pressure distortions.

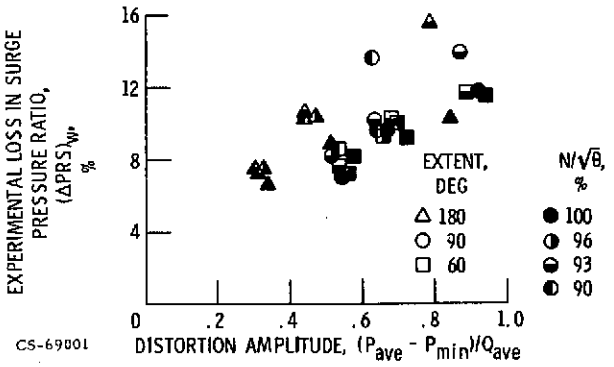

Figure 6. - Loss in J-85 surge pressure ratio (evaluated at a constant corrected airflow) due to circumferential pressure distortions.

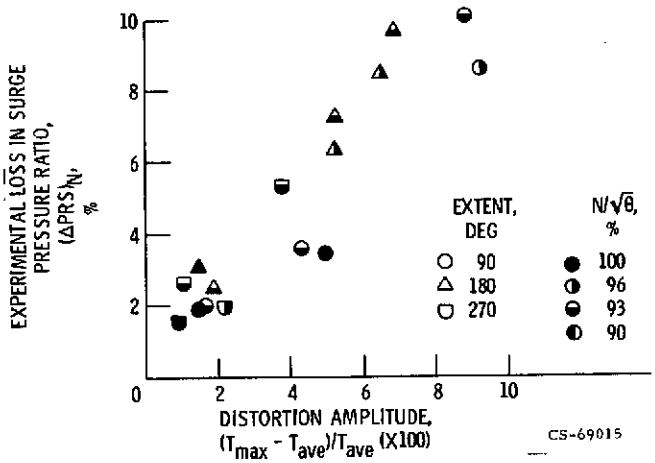

Figure 7. - Loss in J-85 pressure ratio (evaluated at a constant corrected speed) due to circumferential temperature distortions.

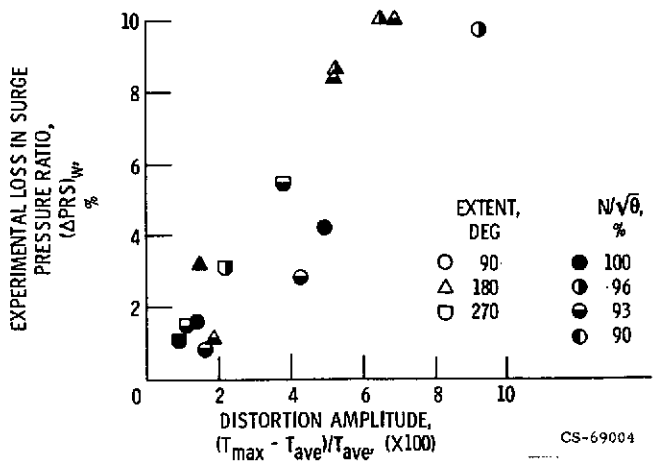

Figure 8. - Loss in surge pressure ratio (evaluated at a constant corrected airflow) due to circumferential temperature distortion.

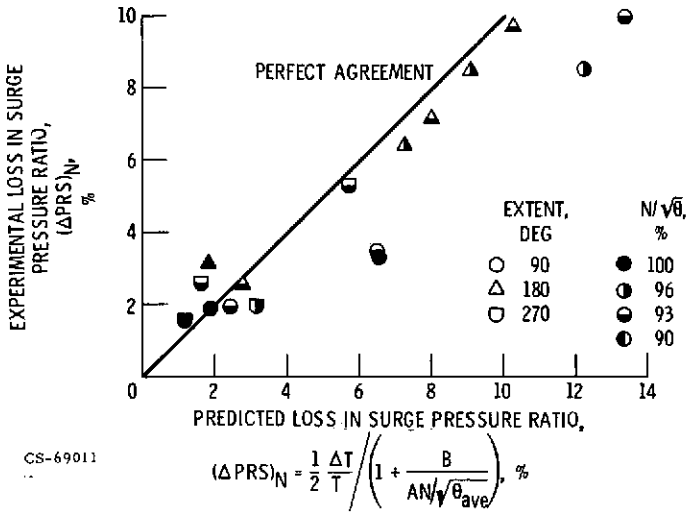

Figure 9. - Comparison of simplified parallel compressor results with experimental data for J-85 circumferential temperature distortion tests.

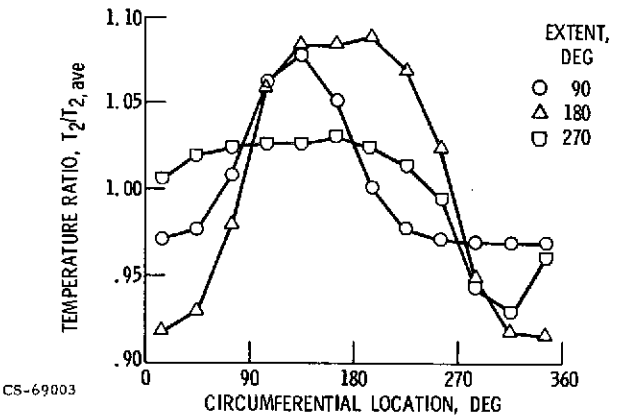

Figure 10. - Circumferential temperature distribution for J-85 temperature distortion.

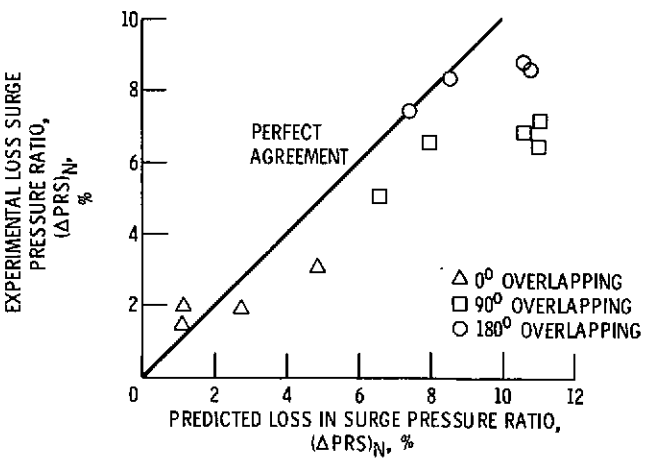

Figure 11. - Comparison of parallel compressor results with experimental data for J-85 combined temperature and pressure distortion.

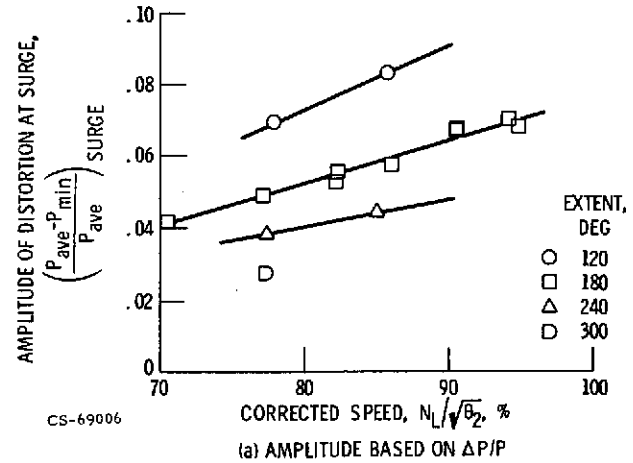

(a) AMPLITUDE BASED ON ΔP/P

Figure 12. - Amplitude of total pressure distortion required to surge the TF30 P-3 turbofan engine.

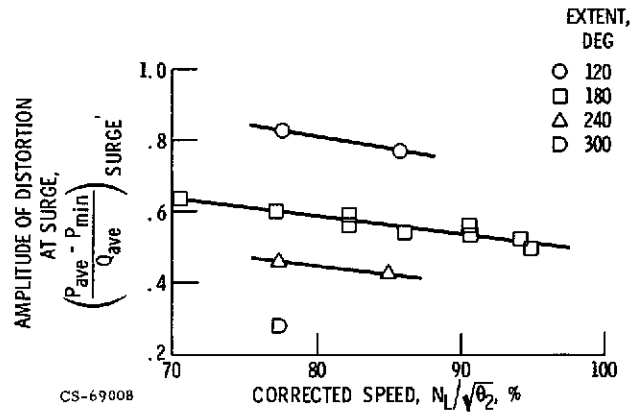

(b) AMPLITUDE BASED ON ΔP/Q

Figure 12. - Concluded.

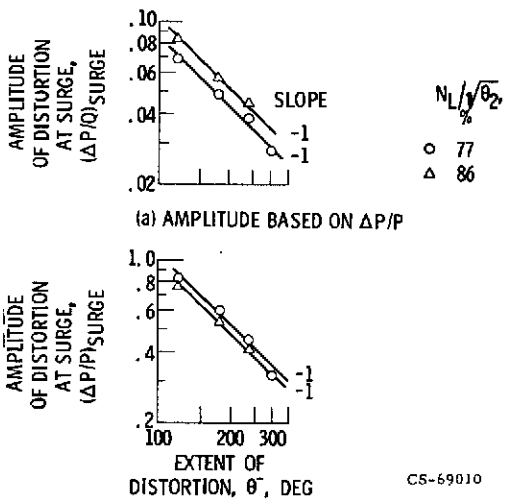

(a) AMPLITUDE BASED ON ΔP/P

(b) AMPLITUDE BASED ON ΔP/Q.

Figure 13. - Relationship between amplitude and extent of TF30 pressure distortions at surge.

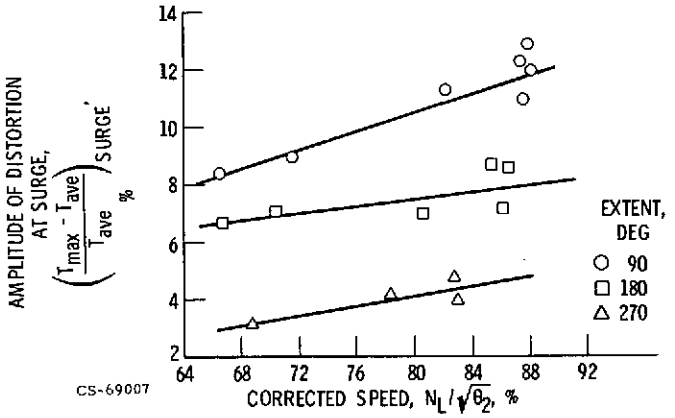

Figure 14. - Amplitude of total temperature distortion required to surge the TF30 P-3 turbofan engine.

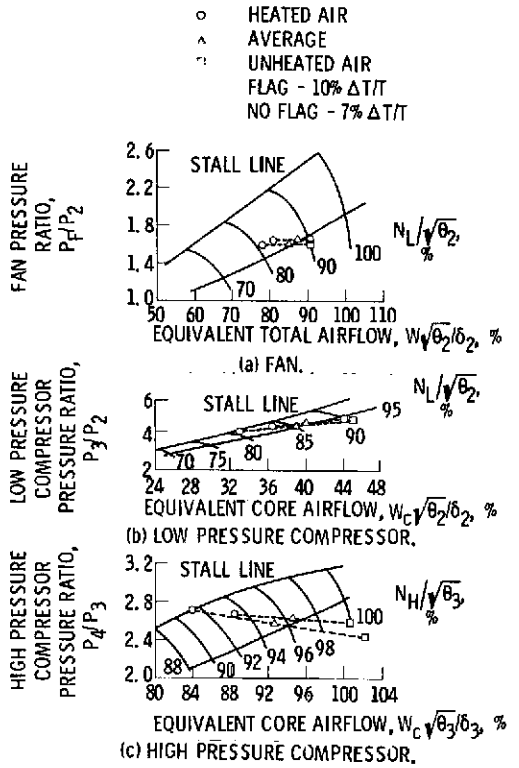

Figure 15. - TF30 operating points predicted by the parallel compressor theory.